Cost-Effective and Self-Textured Gallium-Doped Zinc Oxide Front Contacts for Hydrogenated Amorphous Silicon Thin-Film Solar Cells

2013 Appl. Phys. Express 6 022301

(http://iopscience.iop.org/1882-0786/6/2/022301)

Applied Physics Express 6 (2013) 022301
http://dx.doi.org/10.7567/APEX.6.022301

Cost-Effective and Self-Textured Gallium-Doped Zinc Oxide Front Contacts for Hydrogenated Amorphous Silicon Thin-Film Solar Cells

Shu-Hung Yu[1], Po-Ching Ho[1], Chia-Ling Lee[2], Chien-Chung Bi[2], Chih-Hung Yeh[2], and Chun-Yen Chang[1]*

[1]*Department of Electronics Engineering and Institute of Electronics, National Chiao Tung University, Hsinchu 30010, Taiwan*
[2]*NexPower Technology Corporation, Taichung County 421, Taiwan*
E-mail: cyc@mail.nctu.edu.tw

Received December 13, 2012; accepted January 14, 2013; published online January 29, 2013

We adopt a economical and original method to fabricate self-textured gallium-doped zinc oxide (GZO) front contacts for hydrogenated amorphous silicon (a-Si:H) single-junction solar cells. This technique involves an atmospheric-pressure plasma jet (APPJ) and a dc sputtering process. The electro-optical characteristics of the textured GZO films are mainly controlled by the haze of organosilicon underlayers deposited by the APPJ. The films exhibit an average optical transmittance of about 80% and resistivity below $9.91 \times 10^{-4}\,\Omega\,\mathrm{cm}$. Moreover, compared with flat solar cells, textured cells fabricated on moderate GZO front contacts show 7.9 and 10.9% enhancements in conversion efficiency and short-circuit current density, respectively.

Transparent conductive oxides (TCOs) are essential for silicon-based thin-film solar cells, including hydrogenated amorphous silicon (a-Si:H) single-junction and hydrogenated microcrystalline silicon (μc-Si:H) single-junction solar cells, owing to their outstanding optical and electrical properties.[1)] However, in order to improve the conversion efficiency and stability of silicon-based solar cells, it is necessary to fabricate well-textured TCO substrates to improve light trapping effects in the Si absorbers. Recently, zinc oxides (ZnOs) doped with group III elements have attracted significant attention thanks to their extraordinary electro-optical characteristics and material abundance.[2)] Moreover, ZnO films are more stable than tin-doped indium oxides (ITOs) and fluorine-doped tin oxides (FTOs) in the hydrogen and silane (SiH_4) plasma discharge. Consequently, they are suitable for the manufacture of microcrystalline silicon (μc-Si) and amorphous silicon (a-Si) solar cells.[3,4)] To date, many achievements have been made for textured ZnO substrates. Textured ZnO films achieved by post wet etching are already well known.[5)] Unfortunately, this method creates much waste of raw materials. Self-textured ZnO doped with boron (BZO) has been successfully fabricated by low-pressure chemical vapor deposition (LPCVD) or metal organic chemical vapor deposition (MOCVD).[6,7)] Nevertheless, these techniques have drawbacks in terms of expensive equipment, toxic precursors, and film instability.

In this study, we exhibit an original and cost-effective technique to produce textured gallium-doped ZnO (GZO) front contacts for a-Si:H single-junction solar cells. A bilayer structure of organosilicon/GZO is used to fabricate self-textured GZO films on glass substrates. This bilayer structure is achieved by an atmospheric pressure plasma jet (APPJ) and dc magnetron sputtering. The APPJ system does not need expensive vacuum systems and maintenance which are necessary for low pressure plasma deposition systems.[8–11)] The surface morphology and electro-optical characteristics of the films can be effectively controlled by the haze of organosilicon underlayers. The performance of superstrate-type a-Si:H solar cells fabricated on the different textured GZO front contacts is examined by current–voltage measurements. Finally, external quantum efficiency (EQE) spectra are obtained to demonstrate that the textured GZO films can significantly enhance light trapping in a-Si:H solar cells.

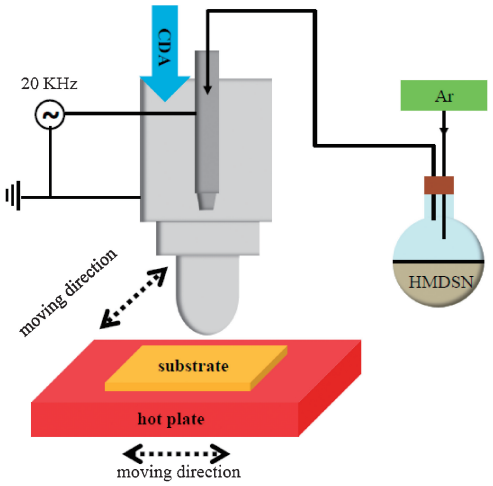

Fig. 1. Schematic diagram of the APPJ construction.

The process flow of fabricating self-textured GZO films is as follows. Firstly, the organosilicon underlayers are deposited on $10 \times 10\,\mathrm{cm}^2$ Corning Eagle XG glass substrates by a 20 kHz APPJ system, as shown in Fig. 1. The RF power is 450 W. The temperature of glass substrates is kept at 75 °C by a hot plate. The hexamethyldisilazane (HMDSN) precursors, easily volatilized at room temperature and low toxic,[12–15)] are carried through the inner tube by Ar carrier gas changed from 120 to 180 sccm. Clean dry air (CDA) is the plasma forming gas, carried through the outside tube, and the flow rate is maintained of 40 slm. The distance between the nozzle and the substrate is 15 mm and the scan speed is 300 mm/s. The 1-μm-thick GZO films are deposited on the organosilicon layers at 100 °C by dc magnetron sputtering. The ceramic target contains ZnO and 3.2 wt % Ga_2O_3. The dc power density is $3\,\mathrm{W/cm}^2$ and the working pressure is 2 mTorr during the sputtering. Finally, all the as-grown textured GZO films are thermally annealed at 500 °C in high vacuum ($< 1 \times 10^{-6}$ Torr) for 5 min to improve the electro-optical properties. Superstrate-type a-Si:H single-junction solar cells are fabricated by plasma-enhanced chemical vapor deposition (PECVD). The thickness of p-type, intrinsic, and n-type silicon layers are 10, 300, and 30 nm, respectively. The surface morphology of organosilicon underlayers and textured GZO films is investigated by atomic force microscopy (AFM) and scanning electron microscopy (SEM),

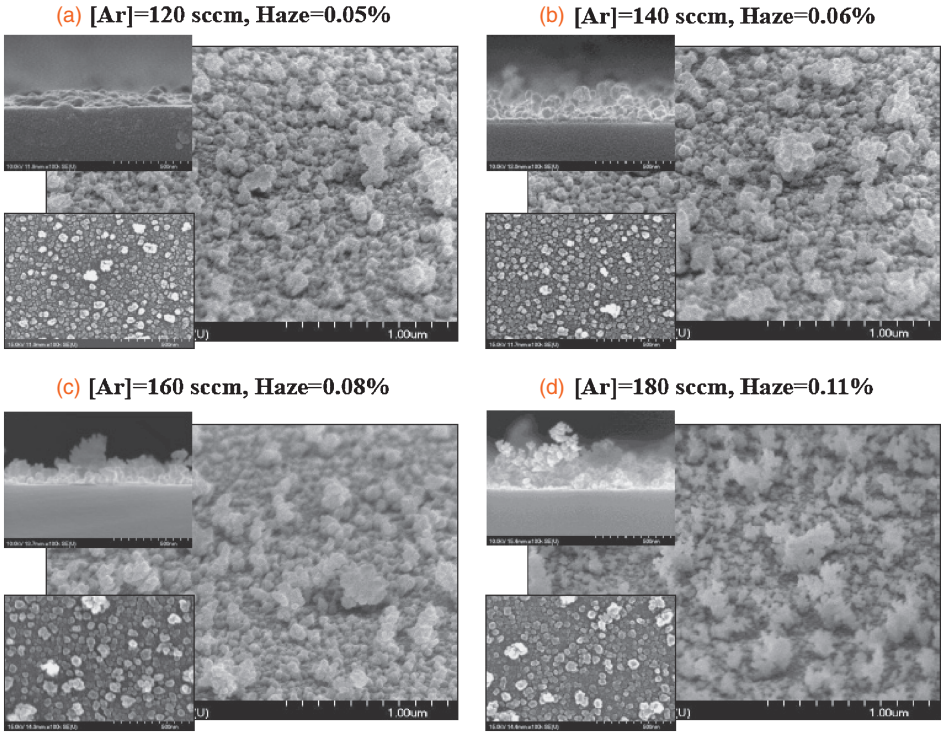

Fig. 2. The SEM images of organosilicon layers deposited with [Ar] of (a) 120, (b) 140, (c) 160, and (d) 180 sccm.

respectively. Optical properties are measured by a UV–visible–NIR spectrophotometer (Hitachi 4100). Electrical characteristics are examined by Hall measurements in the van der Pauw configuration at RT. Current–voltage measurements for a-Si:H solar cells are conducted with a dual light solar simulator (Wacom WXS-220S L2) under an AM1.5G 100 mW/cm^2 illumination. Incident photo-to-current efficiency is measured in the wavelength range of 350–800 nm to evaluate external quantum efficiency (EQE).

Figure 2 shows SEM images of organosilicon layers deposited at different Ar flow rates ([Ar]) increased from 120 to 180 sccm. The film thickness increases from around 200 to around 500 nm with increasing [Ar]. Meanwhile, the organosilicon clusters can also be expanded by increasing [Ar]. According to the results of Benedikt et al., the difference in flow rate between carrier gas and plasma forming gas can induce vortexes and reactive particles inside the tube.[16] More active organosilicon particles are brought onto the substrate with higher [Ar], and therefore they merge into big clusters effectively on the surface. Substantially, the optical roughness of the organosilicon layers can also be controlled by [Ar]. The haze value, measured by a UV–visible–NIR spectrophotometer, at the wavelength of 550 nm rises significantly from 0.05 to 0.11% with increasing [Ar]. Here, organosilicon clusters provide not only light-scattering centers but also the nucleation sites for GZO deposition. Figure 3 shows top-view and tilted SEM images of 1-μm-thick GZO films deposited on different organosilicon layers. The island-like shapes on textured GZO films expand significantly with increasing roughness of organosilicon underlayers. Organosilicon clusters serve as the nucleation sites during the sputtering, and therefore GZO can grow rapidly near the clusters and form these specific textures. According to our observation during the sputtering deposition, the growth rates of all the textured GZO films are about 1.4 times greater than that of the flat ones. Besides, AFM shows that the RMS roughness of textured GZO films increases significantly from 29.0 to 54.4 nm with increasing underlayer haze.

Figure 4 reveals the Hall measurement results of textured GZO films as a function of the RMS roughness. The carrier density shows slight variations with increasing RMS roughness of GZO films. We speculate that the moderate surface roughness of organosilicon layers does not significantly affect the activation of Ga atoms and the carrier density in the films. Hall mobility suffers vast effects from underlayer roughness. In particular, when the haze value exceeds 0.08%, the mobility of GZO drops to 26.0 cm^2 V^{-1} s^{-1}. This mobility degradation is attributed to the presence of a lot of lattice defects in highly textured GZO films.[17] Moreover, there are many valleys on the textured GZO surfaces when the RMS roughness is higher than 48.6 nm, as shown in Fig. 3, which also significantly damage Hall mobility. The resistivity of the textured GZO films increases from 8.14×10^{-4} to 9.91×10^{-4} Ω cm accompanying the decreasing trend of Hall mobility. Figure 5(a) shows the optical transmittance and reflectance spectra of textured GZO films. Most of the films reveal an average transmittance of about 80% in a wide wavelength range. Especially in the near-infrared region, because that these GZO films have the moderate carrier concentration, lower than 10^{21} cm^{-3}, which can prevent the strong absorption from free carriers.[18] By observing the trend of transmittance and reflectance spectra, the absorption in the visible wavelength range becomes more obvious with increasing the RMS roughness. This defect-related absorption results from the optically-assisted electron transition from valance band to trap states in the forbidden gap, and it overwhelms the antireflection effects

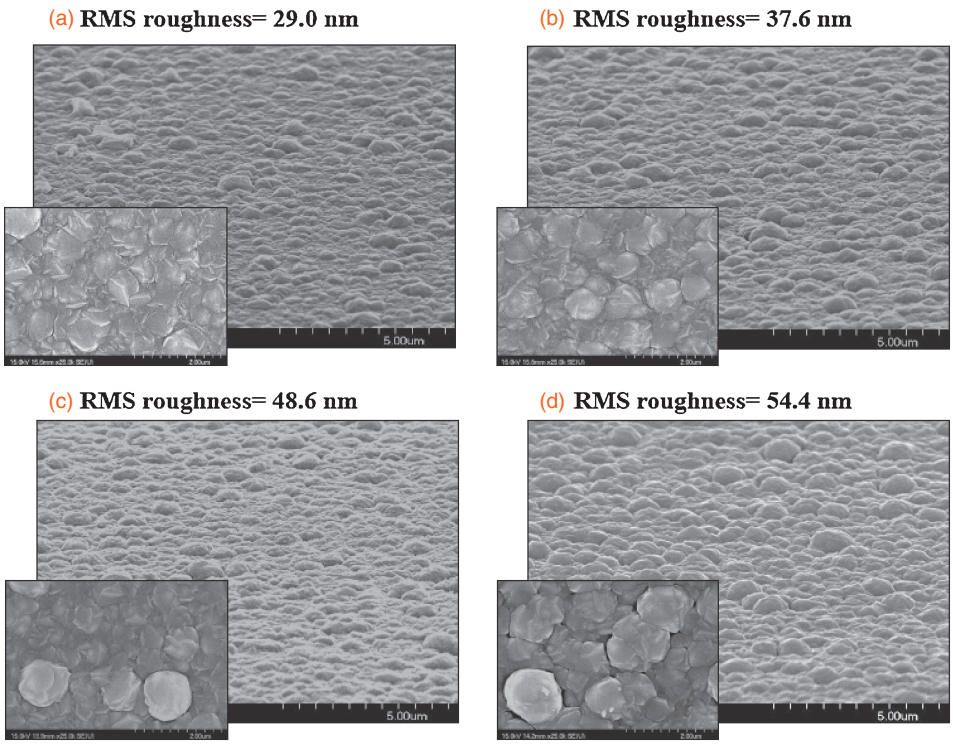

Fig. 3. Top-view and tilted SEM images of textured GZO films with RMS roughness of (a) 29.0, (b) 37.6, (c) 48.6, and (d) 54.4 nm.

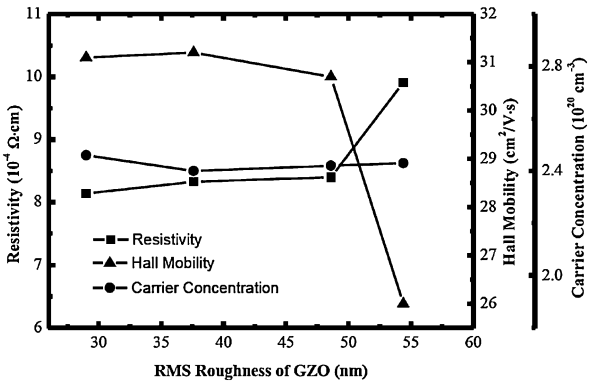

Fig. 4. Resistivity, Hall mobility, and carrier concentration of textured GZO films as a function of RMS roughness.

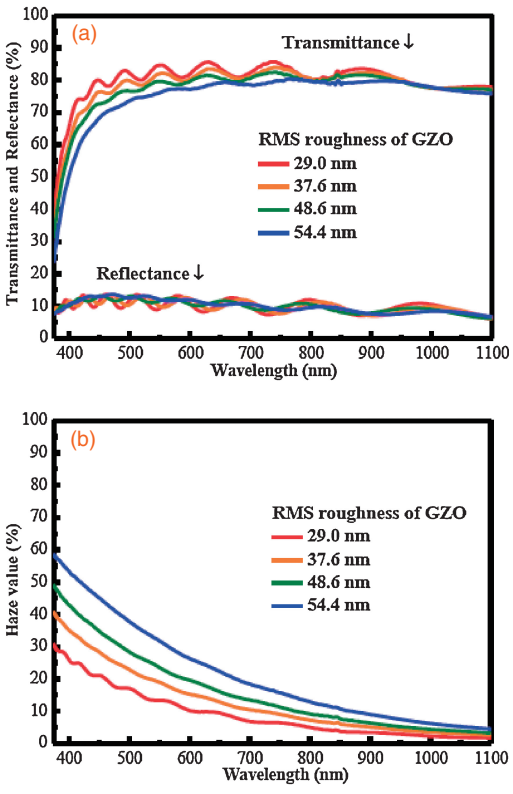

Fig. 5. (a) Optical transmittance and reflectance spectra, and (b) haze values of different textured GZO films in the wavelength range of 375–1100 nm.

from organosilicon and textured GZO films.[19] As shown in Fig. 5(b), the haze value of textured GZO films in a wide wavelength range can be enhanced effectively by increasing the roughness of organosilicon underlayers. In this study, the height haze value of 32% at the wavelength of 550 nm is achieved. Meanwhile, the optical roughness can eliminate the interference phenomenon in the optical transmittance spectra owing to Fabry–Perot resonances within the thick GZO films.

Here, we fabricate superstrate-type a-Si:H single cells on these textured GZO films to evaluate their light trapping capability. The current–voltage characteristics of textured and flat a-Si:H solar cells measured under an AM1.5G 100 mW/cm^2 illumination are shown in Fig. 6. Compared with the flat solar cells, the textured cells fabricated on the GZO front contacts with RMS roughness of 29.0 nm show a 10.9% enhancement in short-circuit current density (J_{sc}) and achieve the conversion efficiency of 7.11%, as shown in the inserted table of Fig. 6. When GZO film RMS roughness is equal to 54.4 nm, the J_{sc} can be further enhanced by 18.2%. However, the open-circuit voltage (V_{oc}) and fill factor (FF)

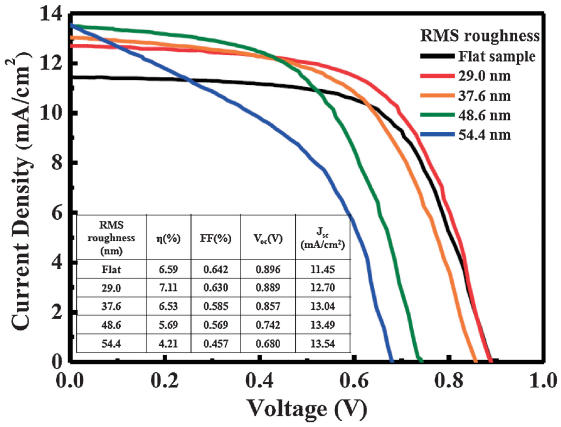

Fig. 6. Current–voltage characteristics and data of a-Si:H solar cells with various GZO front contacts.

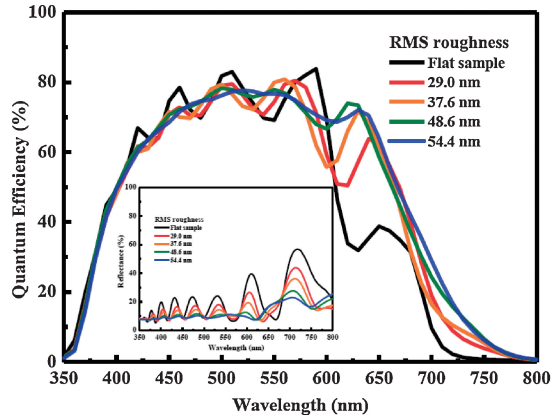

Fig. 7. EQE and reflectance spectra of a-Si:H solar cells with various GZO front contacts.

suffer significant drops when RMS roughness exceeds 29.0 nm. We speculate that highly rough GZO surfaces can cause shunting paths and leakage currents in a-Si:H absorbers, which result in drastic reductions in V_{oc}. Besides, according to the relation between V_{oc} and FF:[20]

$$\mathrm{FF} = 1 - \frac{KT}{qV_{oc}} \ln\left(1 + \frac{qV_m}{KT}\right) - \frac{KT}{qV_{oc}}, \quad (1)$$

where K is Boltzmann's constant, T is the absolute temperature, q is the electron charge, and V_m is the voltage of the maximum output power point in current–voltage characteristics, the shrinkage of V_{oc} can also result in reductions in FF. These results imply that a-Si:H solar cells do not need excessively textured front contacts. EQE and reflectance spectra of flat and textured solar cells in the wavelength range of 350–800 nm are shown in Fig. 7. The incident photo-to-electron conversion efficiency of textured solar cells can get great enhancements in the wavelength range of 600–800 nm. Besides, the textured solar cells reveal significantly suppressed reflectance, as shown in the reflectance spectra inserted in Fig. 7. For the wavelength below 550 nm, the absorption coefficient of a-Si:H is high enough and the trend of suppressed reflectance is due to the anti-reflection near the GZO/Si interface. However, the textured substrates can cause more defective centers near the interfaces between p-type and intrinsic Si layers, which suppress the enhancement of EQE below 550 nm. For the wavelength above 550 nm, the absorption coefficient of a-Si:H is too low to efficiently absorb the incoming light in the thin active layer so the suppressed reflectance mainly results from light-trapping effects. However, the saturated optical absorption of active layers limits the further enhancement of J_{sc} with increasing GZO RMS roughness. The optical interferences due to Fabry–Perot oscillations in thick a-Si:H layers are also eliminated efficiently by these textured structures.

In summary, the economical and self-textured GZO films are produced successfully by depositing organosilicon underlayers through the APPJ in advance. The organosilicon clusters are created purposely to induce island-like textures on the GZO surfaces. Moreover, these GZO films also reveal outstanding electro-optical characteristics and a high haze value. We demonstrate that these textured GZO front contacts can efficiently induce light-trapping effects in a-Si:H single-junction solar cells, especially in the wavelength range above 600 nm. We also demonstrate that a-Si:H solar cells deposited on the well-textured front contacts, with an RMS roughness of 29.0 nm, can achieve the conversion efficiency of 7.11%. In this study, the advantages of the technique for textured TCO substrates are its cost-effectiveness and ease of production, and therefore it has a high potential for application in photovoltaic industrial manufacture.

Acknowledgment This work was supported by the National Science Council of Taiwan under Grant NSC 101-3113-E-009-004.

1) A. V. Shah, H. Schade, M. Vanecek, J. Meier, E. Vallat-Sauvain, N. Wyrsch, U. Kroll, C. Droz, and J. Bailat: Prog. Photovoltaics **12** (2004) 113.
2) M. Boccard, T. Söderström, P. Cuony, C. Battaglia, S. Hänni, S. Nicolay, L. Ding, M. Benkhaira, G. Bugnon, A. Billet, M. Charrière, F. Meillaud, M. Despeisse, and C. Ballif: IEEE J. Photovoltaics **2** (2012) 229.
3) R. Banerjee, S. Ray, N. Basu, A. K. Batabyal, and A. K. Barua: J. Appl. Phys. **62** (1987) 912.
4) H. Sato, T. Minami, and S. Takata: J. Vac. Sci. Technol. A **11** (1993) 2975.
5) O. Kluth, B. Rech, L. Houben, S. Wieder, G. Schöpe, C. Beneking, H. Wagner, A. Löffl, and H. W. Schock: Thin Solid Films **351** (1999) 247.
6) J. Bailat, D. Dominé, R. Schlüchter, J. Steinhauser, S. Fäy, F. Freitas, C. Bücher, L. Feitknecht, X. Niquille, T. Tscharner, A. Shah, and C. Ballif: Conf. Rec. IEEE 4th World Conf. Photovoltaic Energy Convers, 2006, p. 1533.
7) X. L. Chen, B. H. Xu, J. M. Xue, Y. Zhao, C. C. Wei, J. Sun, Y. Wang, X. D. Zhang, and X. H. Geng: Thin Solid Films **515** (2007) 3753.
8) A. Schütze, J. Y. Jeong, S. E. Babayan, J. Park, G. S. Selwyn, and R. F. Hicks: IEEE Trans. Plasma Sci. **26** (1998) 1685.
9) C. Tendero, C. Tixier, P. Tristant, J. Desmaison, and P. Leprince: Spectrochim. Acta, Part B **61** (2006) 2.
10) C. Huang, W. T. Hsu, C. H. Liu, S. Y. Wu, S. H. Yang, T. H. Chen, and T. C. Wei: IEEE Trans. Plasma Sci. **37** (2009) 1127.
11) C. Huang, S. Y. Wu, and Y. C. Chang: IEEE Trans. Plasma Sci. **38** (2010) 1101.
12) S. H. Yang, C. H. Liu, C. H. Su, and H. Chen: Thin Solid Films **517** (2009) 5284.
13) K. Schmidt-Szalowski, Z. Rzanek-Boroch, J. Sentek, Z. Rymuza, Z. Kusznierewicz, and M. Misiak: Plasmas Polym. **5** (2000) 173.
14) D. H. Kuo and D. G. Yang: Thin Solid Films **374** (2000) 92.
15) M. T. Kim and J. Lee: Thin Solid Films **303** (1997) 173.
16) J. Benedikt, V. Raballand, A. Yanguas-Gil, K. Focke, and A. von Keudell: Plasma Phys. Control. Fusion **49** (2007) B419.
17) S. H. Yu, P. C. Ho, T. W. Yang, C. C. Bi, C. H. Yeh, and C. Y. Chang: Electrochem. Solid-State Lett. **1** (2012) 48.
18) K. L. Chopra, S. Major, and D. K. Pandya: Thin Solid Films **102** (1983) 1.
19) P. S. Xu, Y. M. Sun, C. S. Shi, G. F. Q. Xu, and H. B. Pan: Nucl. Instrum. Methods Phys. Res., Sect. B **199** (2003) 286.
20) H. Y. Lee, H.-L. Huang, and C.-T. Lee: Appl. Phys. Express **5** (2012) 122302.